EUROPEAN ORGANIZATION FOR NUCLEAR RESEARCH

CERN-EP/90-34
March 14th, 1990

A Search for Pair-Produced Charged Higgs Bosons in Z^0 Decays

14 March 1990

The ALEPH Collaboration

D. Decamp, B. Deschizeaux, C. Goy, J.-P. Lees, M.-N. Minard

Laboratoire de Physique des Particules (LAPP), IN²P³-CNRS, 74019 Annecy-le-Vieux Cedex, France

J.M. Crespo, M. Delfino, E. Fernandez[1], M. Martinez, R. Miquel, Ll.M. Mir, S. Orteu, A. Pacheco, J.A. Perlas, E. Tubau

Laboratorio de Fisica de Altas Energias, Universidad Autonoma de Barcelona, 08193 Bellaterra (Barcelona), Spain[10]

M.G. Catanesi, M. de Palma, A. Farilla, G. Iaselli, G. Maggi, S. Natali, S. Nuzzo, A. Ranieri, G. Raso, F. Romano, F. Ruggieri, G. Selvaggi, L. Silvestris, P. Tempesta, G. Zito

INFN Sezione di Bari e Dipartimento di Fisica dell' Università, 70126 Bari, Italy

Y. Gao, H. Hu, D. Huang, S. Jin, J. Lin, T. Ruan, T. Wang, W. Wu, Y. Xie, D. Xu, R. Xu, J. Zhang, Z. Zhang, W. Zhao

Institute of High-Energy Physics, Academia Sinica, Beijing, The People's Republic of China[11]

H. Albrecht[2], W.B. Atwood[3], F. Bird, E. Blucher, T.H. Burnett[4], T. Charity, H. Drevermann, Ll. Garrido, C. Grab, R. Hagelberg, S. Haywood, B. Jost, M. Kasemann, G. Kellner, J. Knobloch, A. Lacourt, I. Lehraus, T. Lohse, D. Lüke[2], A. Marchioro, P. Mato, J. May, A. Minten, A. Miotto, P. Palazzi, M. Pepe-Altarelli, F. Ranjard, A. Roth, J. Rothberg[4], H. Rotscheidt, W. von Rüden, R. St.Denis, D. Schlatter, M. Takashima, M. Talby[5], H. Taureg, W. Tejessy, H. Wachsmuth, S. Wheeler, W. Wiedenmann, W. Witzeling, J. Wotschack

European Laboratory for Particle Physics (CERN), 1211 Geneva 23, Switzerland

Z. Ajaltouni, M. Bardadin-Otwinowska, A. Falvard, P. Gay, P. Henrard, J. Jousset, B. Michel, J-C. Montret, D. Pallin, P. Perret, J. Proriol, F. Prulhière

Laboratoire de Physique Corpusculaire, Université Blaise Pascal, IN²P³-CNRS, Clermont-Ferrand, 63177 Aubière, France

J.D. Hansen, J.R. Hansen, P.H. Hansen, R. Mø llerud, G. Petersen

Niels Bohr Institute, 2100 Copenhagen, Danmark[12]

E. Simopoulou, A. Vayaki

Nuclear Research Center Demokritos (NRCD), Athens, Greece

J. Badier, A. Blondel, G. Bonneaud, J. Bourotte, F. Braems, J.C. Brient, M.A. Ciocci, G. Fouque, R. Guirlet, A. Rougé, M. Rumpf, R. Tanaka, H. Videau, I. Videau[1]

Laboratoire de Physique Nucléaire et des Hautes Energies, Ecole Polytechnique, IN²P³-CNRS, 91128 Palaiseau Cedex, France

D.J. Candlin

Department of Physics, University of Edinburgh, Edinburgh EH9 3JZ, United Kingdom[13]

A. Conti, G. Parrini

Dipartimento di Fisica, Università di Firenze, INFN Sezione di Firenze, 50125 Firenze, Italy

M. Corden, C. Georgiopoulos, J.H. Goldman, M. Ikeda, J. Lannutti, D. Levinthal[18], M. Mermikides, L. Sawyer, G. Stimpfl

Supercomputer Computations Research Institute and Dept. of Physics, Florida State University, Tallahassee FL 32306, USA[15,16,17]

A. Antonelli, R. Baldini, G. Bencivenni, G. Bologna[6], F. Bossi, P. Campana, G. Capon, V. Chiarella, G. De Ninno, B. D'Ettorre-Piazzoli[7], G. Felici, P. Laurelli, G. Mannocchi[7], F. Murtas, G.P. Murtas, G. Nicoletti, P. Picchi[6], P. Zografou

Laboratori Nazionali dell'INFN (LNF-INFN), 00044 Frascati, Italy

B. Altoon, O. Boyle, A.W. Halley, I. ten Have, J.L. Hearns, I.S. Hughes, J.G. Lynch, W.T. Morton, C. Raine, J.M. Scarr, K. Smith[1], A.S. Thompson

Department of Physics and Astronomy, University of Glasgow, Glasgow G12 8QQ, United Kingdom[13]

B. Brandl, O. Braun, R. Geiges, C. Geweniger[1], P. Hanke, V. Hepp, E.E. Kluge, Y. Maumary, M. Panter, A. Putzer, B. Rensch, A. Stahl, K. Tittel, M. Wunsch

Institut für Hochenergiephysik, Universität Heidelberg, 6900 Heidelberg, Fed. Rep. of Germany[19]

A.T. Belk, R. Beuselinck, D.M. Binnie, W. Cameron[1], M. Cattaneo, P.J. Dornan, S. Dugeay, R.W. Forty, A.M. Greene, J.F. Hassard, S.J. Patton, J.K. Sedgbeer, G. Taylor, I.R. Tomalin, A.G. Wright

Department of Physics, Imperial College, London SW7 2BZ, United Kingdom[13]

P. Girtler, D. Kuhn, G. Rudolph

Institut für Experimentalphysik, Universität Innsbruck, 6020 Innsbruck, Austria[21]

C.K. Bowdery[1], T.J. Brodbeck, A.J. Finch, F. Foster, G. Hughes, N.R. Keemer, M. Nuttall, B.S. Rowlingson, T. Sloan, S.W. Snow

Department of Physics, University of Lancaster, Lancaster LA1 4YB, United Kingdom[13]

T. Barczewski, L.A.T. Bauerdick, K. Kleinknecht[1], B. Renk, S. Roehn, H.-G. Sander, M. Schmelling, F. Steeg

Institut für Physik, Universität Mainz, 6500 Mainz, Fed. Rep. of Germany [19]

J-P. Albanese, J-J. Aubert, C. Benchouk, A. Bonissent, D. Courvoisier, F. Etienne, E. Matsinos, S. Papalexiou, P. Payre, B. Pietrzyk[1], Z. Qian

Centre de Physique des Particules, Faculté des Sciences de Luminy, IN^{2}P^3-CNRS, 13288 Marseille, France

W. Blum, P. Cattaneo, G. Cowan, B. Dehning, H. Dietl, M. Fernandez-Bosman, D. Hauff, A. Jahn, E. Lange, G. Lütjens, G. Lutz, W. Männer, H-G. Moser, Y. Pan, R. Richter, A.S. Schwarz, R. Settles, U. Stiegler, U. Stierlin, J. Thomas, G. Waltermann

Max-Planck-Institut für Physik und Astrophysik, Werner-Heisenberg-Institut für Physik, 8000 München, Fed. Rep. of Germany[19]

V. Bertin, G. de Bouard, J. Boucrot, O. Callot, X. Chen, A. Cordier, M. Davier, G. Ganis, J.-F. Grivaz, Ph. Heusse, P. Janot, V. Journé, D.W. Kim, J. Lefrançois, A.-M. Lutz, J.-J. Veillet, F. Zomer

Laboratoire de l'Accéléateur Linéaire, Université de Paris-Sud, IN^{2}P^3-CNRS, 91405 Orsay Cedex, France

S.R. Amendolia, G. Bagliesi, G. Batignani, L. Bosisio, U. Bottigli, C. Bradaschia, I. Ferrante, F. Fidecaro, L. Foà[1], E. Focardi, F. Forti, A. Giassi, M.A. Giorgi, F. Ligabue, A. Lusiani, E.B. Mannelli, P.S. Marrocchesi, A. Messineo, F. Palla, G. Sanguinetti, S. Scapellato, J. Steinberger, R. Tenchini, G. Tonelli, G. Triggiani

Dipartimento di Fisica dell'Università, INFN Sezione di Pisa, e Scuola Normale Superiore,56010 Pisa, Italy

J.M. Carter, M.G. Green, P.V. March, T. Medcalf, M.R. Saich, J.A. Strong[1], R.M. Thomas, T. Wildish
Department of Physics, Royal Holloway & Bedford New College, University of London, Surrey TW20 OEX, United Kingdom[13]

D.R. Botterill, R.W. Clifft, T.R. Edgecock, M. Edwards, S.M. Fisher, J. Harvey, T.J. Jones, P.R. Norton, D.P. Salmon, J.C. Thompson
Particle Physics Dept., Rutherford Appleton Laboratory, Chilton, Didcot, OXON OX11 OQX, United Kingdom[13]

B. Bloch-Devaux, P. Colas, C. Klopfenstein, E. Lançon, E. Locci, S. Loucatos, L. Mirabito, E. Monnier, P. Perez, F. Perrier, J. Rander, J.-F. Renardy, A. Roussarie, J.-P. Schuller
Département de Physique des Particules Élémentaires, CEN-Saclay, 91191 Gif-sur-Yvette Cedex, France[20]

J.G. Ashman, C.N. Booth, F. Combley, M. Dinsdale, J. Martin, D. Parker, L.F. Thompson
Department of Physics, University of Sheffield, Sheffield S3 7RH, United Kingdom[13]

S. Brandt, H. Burkhardt, C. Grupen, H. Meinhard, E. Neugebauer, U. Schäfer, H. Seywerd
Fachbereich Physik, Universität Siegen, 5900 Siegen, Fed. Rep. of Germany[19]

B. Gobbo, F. Liello, E. Milotti, F. Ragusa[8], L. Rolandi[1]
Dipartimento di Fisica, Università di Trieste e INFN Sezione di Trieste, 34127 Trieste, Italy

T. Barklow, L. Bellantoni, J.F. Boudreau, D. Cinabro, J.S. Conway, D.F. Cowen, Z. Feng, Y.-S. Gao, J.L. Harton, J. Hilgart, R.C. Jared[9], R.P. Johnson, B.W. LeClaire, Y.B. Pan, T. Parker, J.R. Pater, Y. Saadi, V. Sharma, A.M. Walsh, J.A. Wear, F.V. Weber, Sau Lan Wu, S.T. Xue, G. Zobernig
Department of Physics, University of Wisconsin, Madison, WI 53706, USA [14]

(Submitted to Phys. Lett. B)

---

[1] Now at CERN.
[2] Permanent address: DESY, Hamburg, Fed. Rep. of Germany.
[3] On leave of absence from SLAC, Stanford, CA 94309, USA.
[4] On leave of absence from University of Washington, Seattle, WA 98195, USA.
[5] Also Centre de Physique des Particules, Faculté des Sciences, Marseille, France
[6] Also Istituto di Fisica Generale, Università di Torino, Torino, Italy.
[7] Also Istituto di Cosmo-Geofisica del C.N.R., Torino, Italy.
[8] Now at INFN Milano.
[9] Permanent address: LBL, Berkeley, CA 94720, USA.
[10] Supported by CAICYT, Spain.
[11] Supported by the National Science Foundation of China.
[12] Supported by the Danish Natural Science Research Council.
[13] Supported by the UK Science and Engineering Research Council.
[14] Supported by the US Department of Energy, contract DE-AC02-76ER00881.
[15] Supported by the US Department of Energy, contract DE-FG05-87ER40319.
[16] Supported by the NSF, contract PHY-8451274.
[17] Supported by the US Department of Energy, contract DE-FC0S-85ER250000.
[18] Supported by SLOAN fellowship, contract BR 2703.
[19] Supported by the Bundesministerium für Forschung und Technologie, Fed. Rep. of Germany.
[20] Supported by the Institut de Recherche Fondamentale du C.E.A..
[21] Supported by Fonds zur Förderung der wissenschaftlichen Forschung, Austria.

Abstract

A search for pair-produced charged Higgs bosons in decays of the Z^0 has been performed using the ALEPH detector at LEP for the decay channels $H^+ H^- \to \nu\overline{\tau}\ \overline{\nu}\tau$, $H^+ H^- \to \nu\tau\ cs$ and $H^+ H^- \to c\overline{s}\ \overline{c}s$. Searches for two additional decay channels in which cs is replaced by cb were also performed. With 1.17 pb^{-1} of integrated luminosity, corresponding to about 25000 hadronic decays of the Z^0, the charged Higgs has been excluded at 95% C.L. in the mass range 7.6 to 43.0 GeV for $BR[H^\pm \to \nu\tau] = 100\%$, 8.3 to 40.6 GeV for $BR[H^\pm \to \nu\tau] = BR[H^\pm \to cs] = 50\%$, and 14.4 to 35.4 GeV for $BR[H^\pm \to cs] = 100\%$. With cs replaced by cb, the charged Higgs has been excluded at 95% C.L. in the mass range 12.0 to 40.7 GeV for $BR[H^\pm \to \nu\tau] = BR[H^\pm \to cb] = 50\%$, and 16.2 to 35.7 GeV for $BR[H^\pm \to cb] = 100\%$.

1 Introduction

The minimal formulation of the Standard Model of electroweak interactions [1] uses a single doublet of complex fields to provide, via the Higgs mechanism [2], masses for the $W^{\pm}$ and Z^0 bosons [3]. In this formulation there is a single massive scalar, the H^0, whose mass is not specified by the theory and which has been recently excluded in the region 32 Mev $< M_{H^0} <$ 24 GeV [4]. However, there is no reason to believe that the Higgs sector is not richer in structure. Non-minimal Higgs sectors may play important roles in such diverse areas as electroweak CP violation [5], the suppression of strong CP violation [6], the generation of neutrino masses [7], and $B^0\overline{B^0}$ mixing [8], and they are an essential element of supersymmetric theories [9]. Models in which there are two or more doublets have $\rho_{\rm tree} = M_W^2/(M_{Z^0}^2\cos^2\theta_W) = 1$ and also allow the absence of flavor-changing neutral currents to be readily arranged [10].

In this letter, the minimal extension of the Standard Model from one having a single complex doublet to one having two such doublets is considered. This extra doublet introduces four additional degrees of freedom and hence four additional physical Higgs particles, bringing the total number of such particles to five, denoted by H^0, h^0, A^0, H^+ and H^-. For the last two of these, a partial width for pair production from Z^0 decay may be obtained without any further specification of the model. This partial width is [11]

$$\Gamma[Z^0 \to H^+H^- \,] \;=\; \frac{G_f M_{Z^0}^3}{6\sqrt{2}\pi}\left(\frac{1}{2}-\sin^2\theta_W\right)^2 \beta_{H^\pm}^3\,, \qquad (1)$$

where $\beta_{H^\pm} = \sqrt{1-4M_{H^\pm}^2/s}$. This gives, for example, a branching ratio of 0.26% for $M_{H^\pm} = 35$ GeV at $s = M_{Z^0}^2$.

The decay rate of the charged Higgs into fermions is given by [12]

$$\Gamma(H^\pm \to \nu_l l) \;=\; \frac{G_f\sqrt{2}}{8\pi} M_{H^\pm}\, m_l^2 \tan^2\beta \qquad (2)$$

$$\Gamma(H^\pm \to u_{i=1,2} d_{j=1,2,3}) \;=\; \frac{G_f\sqrt{2}}{8\pi} M_{H^\pm}\, 3|V_{ij}|^2 \left[m_i^2\cot^2\beta + m_j^2\tan^2\beta\right], \qquad (3)$$

where $l = (e, \mu, \tau)$, u = up-type quarks, d = down-type quarks and $\tan\beta = v_2/v_1$ is the ratio of the vacuum expectation values. Hence, in the mass range explored in this letter the following processes will dominate:

$$\mathrm{Z}^0 \longrightarrow \begin{cases} H^+, H^- \to \nu\overline{\tau}, \overline{\nu}\tau \\ H^+, H^- \to \nu\overline{\tau}, \overline{c}s \quad \text{or} \quad H^+, H^- \to \nu\overline{\tau}, \overline{c}b \\ H^+, H^- \to c\overline{s}, \overline{c}s \quad \text{or} \quad H^+, H^- \to c\overline{b}, \overline{c}b. \end{cases} \tag{4}$$

Searches for these processes are presented in sections 3,4, and 5, respectively. The two hadronic decay modes $\mathrm{H}^\pm \to cs$ and $\mathrm{H}^\pm \to cb$ are required to satisfy identical selection criteria, and for each of the processes above which involve hadronic decays two distinct limit contours are derived. From eq. (3), the relative rate $\Gamma(cb)/\Gamma(cs) \simeq 0.01$ to 0.05 for $\tan\beta \simeq 1$, and 0.6 to 2.4 for $\tan\beta \gg 1$, using quark masses and Kobayashi-Maskawa matrix elements as given in ref. 15.

These analyses have been performed using the data obtained by the ALEPH detector at LEP from September to December, 1989, collected at the Z^0 peak and in a region ± 3 GeV around it. A total of 1.17 pb^{-1} of integrated luminosity, corresponding to about 25000 hadronic Z^0 decays, have been used.

2 The ALEPH Detector

The ALEPH detector has been described in detail elsewhere [14]. Briefly, the parts of the detector relevant to the analyses presented in this letter are: the cylindrical inner tracking chamber (ITC), extending from 13 to 29 cm in radius and providing up to 8 coordinates in azimuth and radius; the cylindrical time projection chamber (TPC), extending to 180 cm in radius and providing up to 21 three-dimensional coordinates; the electromagnetic calorimeter (ECAL), having 45 lead sheet/proportional wire chamber layers and 74000 cathode pad towers arranged in a projective geometry; and the hadron calorimeter (HCAL), having 23 iron slab/streamer tube layers and 4600 projective cathode pad towers. The HCAL which also serves as the iron return yoke of the magnet, which is a 1.5 T superconducting solenoid located between the ECAL and

HCAL barrels. The luminosity calorimeter (LCAL) provides energy and position measurements of the e^+e^- pairs coming from small-angle Bhabha scattering and is similar in construction to the ECAL.

The readout of the detector is triggered independently by several separate conditions, three of which are relevant for this study. The first requires an energy deposit of at least 6.6 GeV in the barrel of the ECAL, or at least 3.7 GeV in one of the endcaps, or at least 1.5 GeV in each of the endcaps. The second independent trigger demands that there be an ITC track (defined as a signal in at least 5 of the 8 cylindrical wire layers recording ionization from charged particles) in azimuthal coincidence with a deposit of at least 1.3 GeV in the ECAL. The third independent trigger requires an ITC track in azimuthal coincidence with a signal penetrating at least 40 cm of iron in the HCAL.

3 Search for H^+H^- decaying to $\nu\overline{\tau}\ \overline{\nu}\tau$

In the decay channel $H^+ H^- \rightarrow \nu\overline{\tau}\ \overline{\nu}\tau$, the two final states considered have "good" charged particles in 1-on-1 and 3-on-1 topologies, corresponding to roughly 75% and 23% of all the possible tau-tau decay modes, respectively. A "good" charged particle is defined as one making an angle α with the beam axis such that $|\cos\alpha| < 0.95$, having at least 4 TPC coordinates, $|d_0| < 2$ cm, $|z_0| < 10$ cm, and a momentum measured by the ITC and TPC greater than 2 GeV. Here, $|d_0|$ is defined as the distance of closest approach to the interaction point in the plane perpendicular to the beam axis and z_0 is defined as the coordinate along the beam with respect to the interaction point. Only those charged particles which meet these criteria are used in this analysis. Events are not kept if they have additional charged particles which do not satisfy the above criteria.

Events with a 3-on-1 topology are kept only if the invariant mass of the three most closely clustered charged particles is less than 2 GeV, consistent with having come from the decay of a tau. In this topology, the most isolated charged particle (see eq. (5)) is

chosen as the daughter of the one-prong decay. Events having a total invariant mass less than 2 GeV are not kept because the simulation of events due to two-photon exchange (henceforth called "2γ" events) is not well understood in this region.

Defining the decay axes as the individual charged particle momenta for the one-prong tau decays, and as the sum of the momenta of the charged particles for the three-prong tau decay, the following quantities are calculated:

1. the angle between the decay axes $\theta_{\rm axes}$;
2. the projection of $\theta_{\rm axes}$ onto the plane perpendicular to the beam axis $\theta_{\rm proj}$;
3. the vector sum of the charged particles' momenta transverse to the beam axis $p_t = |\sum \vec{p}_\perp|$.

Background from $Z^0 \to l^+l^-(\gamma)$ events is reduced by the requirement $\cos\theta_{\rm axes} > -0.9$. Fig. 1 shows the distribution of $\theta_{\rm axes}$ for the data, the simulated background, and a simulated 40.0 GeV charged Higgs signal for those events which pass the 1-on-1 or 3-on-1 topology requirement and the invariant mass criteria. In this figure, the simulated background and the simulated charged Higgs signal are normalized to the integrated luminosity of the data. Both 2γ and $Z^0 \to l^+l^-(\gamma)$ backgrounds are reduced by requiring $p_t > 7$ GeV. Further reduction in 2γ background is achieved by requiring $\cos\theta_{\rm proj} > -0.99$, and further reduction in $Z^0 \to l^+l^-(\gamma)$ background comes from the veto of events with a clustered energy deposit greater than 5 GeV in the ECAL or LCAL outside a cone of half-angle 20° centered on each decay axis. Since the charged Higgs signal process is rich in neutrinos, the total energy in the ECAL is required to be less than $0.45\sqrt{s}$. With these event selection criteria, no events are observed in the data.

In this analysis and in the analyses which follow, all simulated events are made using Monte Carlo methods which include triggering and detector efficiencies, detector geometry and initial-state radiation, and all are processed by the same reconstruction

and analysis programs used for the data. The simulation of the tau decay follows recently measured branching fractions [15]. Monte Carlo methods are used to simulate the background due to $Z^0 \to l^+l^-(\gamma)$, 2γ, and $Z^0 \to q\bar{q}(g)$ processes [16,17]. Based on these simulations, 1.46±0.33 events are expected to satisfy all the selection criteria.

Since there is no evidence for a signal in the accessible $H^\pm$ mass range, a 95% C.L. limit is set at 3.0 signal events, assuming Poisson statistics. The contour of the excluded mass region is given in fig. 2 as a function of BR[$H^\pm \to \nu\tau$], the leptonic branching ratio of the charged Higgs. Table 1 shows the number of expected signal (μ_s) and background (μ_b) events and the signal efficiency (ϵ) at several values of $M_{H^\pm}$.

4 Search for H^+H^- decaying to $\nu\tau\ cs$ or $\nu\tau\ cb$

The characteristic topology for the decay channels $H^+\ H^- \to \nu\tau\ cs$ and $H^+\ H^- \to \nu\tau\ cb$ is a two-jet-like system plus an acoplanar isolated charged particle coming from the hadronic decay of one charged Higgs and the leptonic decay of the other, respectively. Missing energy and momentum result from undetected neutrinos. Since the signature contains jets, only events which pass Z^0 multihadronic decay selection criteria are accepted. These criteria are that each event must have at least five "good" charged particles and the total energy in these charged particles must exceed 10% of the center-of-mass energy. A good charged particle is defined using the same criteria as in section 3, but without any minimum momentum requirement. Only charged particles satisfying these criteria are used in this analysis. In this analysis and in the analysis in the next section, LUND 6.3 Parton Shower [16] is used to simulate the hadronization process in the $H^\pm$ decays.

The most isolated charged particle in an event is selected as follows: for each charged particle i the isolation parameter ρ_i is calculated by clustering [18] all charged particles

except the ith into N jets. The quantity ρ_i is defined as [19]

$$\rho_i = \min_{j=1,N} \left\{ \sqrt{2E_i(1-\cos\theta_{ij})} \right\}, \quad (5)$$

where E_i is the energy in GeV of the ith charged particle and θ_{ij} is the angle between the ith charged particle and the axis of the jth jet. The most isolated charged particle in an event has the largest value of ρ_i. Only events whose most isolated charged particle has a momentum greater than 1.5 GeV are accepted.

Once the most isolated charged particle is selected, all the remaining charged particles are grouped into two jets. Two characteristic angles are defined for the resulting topology:

1. the angle ϕ between the isolated charged particle and the normal to the plane containing the two jets;

2. the angle $\theta_{\rm jets}$ between the two jets.

Missing momentum in the Higgs signal causes the isolated charged particle to be acoplanar with respect to the two-jet system, therefore $|\cos\phi| > 0.25$ is required. To reduce two-jet background, $\theta_{\rm jets} < 135°$ is required.

For each event satisfying the topology selection, the following quantities are calculated:

1. the boosted sphericity S^b defined, in the rest frame of the two-jet system, as the sphericity of all the charged particles except the most isolated one;

2. the decay angle θ^d, defined, in the rest frame of the two-jet system, as the angle the boosted jets make with the direction of the two-jet system in the Z^0 rest frame;

3. the sum of the energy deposited in the ECAL, $E_{\rm ECAL}$, and the sum of the energy deposited in the LCAL, $E_{\rm LCAL}$;

4. the direction of the thrust axis of the event;

5. the vector sum of the charged particles' momenta transverse to the beam axis $p_t = |\sum \vec{p}_\perp|$.

In the rest frame of the hadronically-decaying Higgs, the two-jet system is well collimated and therefore $S^b < 0.2$ is required. Since the $H^\pm$ decays isotropically in its rest frame, in contrast to gluon radiation from quarks, $\cos\theta^d < 0.6$ is required. To remove any event which may mimic an isolated charged particle topology by virtue of having some of its charged particles escape undetected, the thrust axis must make an angle $\theta_{\rm thr}$ with the beam axis such that $|\cos\theta_{\rm thr}| < 0.9$, and $E_{\rm LCAL}$ is required to be less than 3 GeV. To select events with missing momentum and energy, $p_t > 6$ GeV and $E_{\rm ECAL} < 35$ GeV are required. With these selection criteria, no events are observed in the data. Fig. 3 shows the distribution of p_t for the data, the simulated background, and a simulated 37.5 GeV charged Higgs signal for events satisfying all selection criteria except $p_t > 6$ GeV. The simulated background and the simulated charged Higgs signal are normalized to the integrated luminosity of the data.

Since there is no evidence for a signal in the accessible $H^\pm$ mass range, a 95% C.L. limit is set at 3.0 signal events as in section 3. The contour of the excluded mass region is given in fig. 2 as a function of BR[$H^\pm \to cs$] and in fig. 4 as a function of BR[$H^\pm \to cb$], the hadronic branching ratios of the charged Higgs. Table 1 shows the number of expected signal (μ_s) and background (μ_b) events, and the signal efficiency (ϵ) for several values of $M_{\rm H^\pm}$. The quantities μ_s and μ_b are obtained by counting the number of simulated $Z^0 \to q\bar{q}(g)$ events which fulfill all the selection criteria and have a reconstructed mass lying in a region $\pm\sigma_M$ around each value of $M_{\rm H^\pm}$ in the table, where $\sigma_M \simeq 2.5$ GeV is the resolution for the reconstructed mass.

5 Search for H^+H^- decaying to $c\bar{s}\ \bar{c}s$ or $c\bar{b}\ \bar{c}b$

In the decay channels $H^+ H^- \to c\bar{s}\ \bar{c}s$ and $H^+ H^- \to c\bar{b}\ \bar{c}b$, the final states have a four-jet topology and hence only events passing the Z^0 multihadronic decay selection criteria described in section 4 are accepted. Only charged particles satisfying the "good" charged particle criteria described in section 4 are used in this analysis.

To remove a large fraction of the $Z^0 \to q\bar{q}(g)$ background, only events with an aplanarity greater than 0.02 are accepted. The charged particles are then clustered into at least two jets [21]. Events having less than four jets or more than five jets are re-clustered [22] so that they have exactly four jets. Five-jet events are made into four-jet events by merging the jet having the smallest energy with the jet closest to it spatially. This procedure provides a better mass resolution than re-clustering for large Higgs masses where gluon radiation is a more frequent occurrence. Jets whose charge magnitude is greater than 2, or whose charged multiplicity is less than 3, are considered to be poorly reconstructed and therefore the corresponding event is removed. From the observed jet velocities $\vec{\beta}_{\rm jet}$, calculated by assigning all charged particles the mass of the charged pion, the energies $E_{\rm jet}$ of the individual jets are recalculated [23] by solving the equations of energy and momentum conservation

$$\sum_{\rm jet=1}^{4} \tilde{E}_{\rm jet} = E_{\rm cm} \quad \text{and} \quad \sum_{\rm jet=1}^{4} \tilde{E}_{\rm jet}\vec{\beta}_{\rm jet} = 0. \tag{6}$$

Events with any jet having a negative recalculated energy are removed. Also, events with any jet having a recalculated energy $\tilde{E}_{\rm jet}$ differing greatly from its original observed value $E_{\rm jet}$, as defined by

$$0.01\ \text{GeV} < \frac{\tilde{E}_{\rm jet}}{E_{\rm jet}}|\tilde{E}_{\rm jet} - E_{\rm jet}| < 100.0\ \text{GeV}, \tag{7}$$

are removed. For the remainder of this analysis, the recalculated jet energies are used.

In each event there are three possible jet-jet pairings, but since the charged Higgs have equal masses only the jet-jet pairing minimizing

$$\left|\tilde{E}_i + \tilde{E}_j - E_{\rm cms}/2\right| \tag{8}$$

is taken, where i, j denote two of the four available jets. For the chosen pairing, with i, j, k, l denoting the individual jets and ij and kl denoting the two jet-pair systems, the following quantities are then calculated:

1. the production angle θ^p, defined as the acute angle between the jet-pair system directions and the beam axis;

2. the invariant masses M_{ij} and M_{kl} of the two jet-pair systems;

3. the two opening angles $\theta_{ij}^{\rm open}$ and $\theta_{kl}^{\rm open}$, defined as the angles made between the jets in each jet-pair system in the Z^0 rest frame;

4. the two decay angles θ_{ij}^d (θ_{kl}^d), defined, in the $ij(kl)$ rest frame, as the angles the boosted jets $i, j(k, l)$ make with the $ij(kl)$ direction in the Z^0 rest frame;

5. the boosted sphericities $S_{ij}^b(S_{kl}^b)$, defined as the sphericities in the $ij(kl)$ rest frame.

In contrast to $Z^0 \to q\overline{q}(g)$ decays, $Z^0 \to H^+H^-$ decays follow a $\sin^2\theta$ distribution, and therefore $\theta^p > 60°$ is required. The two charged Higgs particles have the same mass, and therefore $|M_{ij} - M_{kl}| < 4$ GeV $\simeq 2\sigma_{\overline{M}}$ is required, where $\sigma_{\overline{M}}$ is the resolution for the average reconstructed mass, $\frac{1}{2}(M_{ij} + M_{kl})$. For the same reason, the opening angles should be nearly the same, hence $|\theta_{ij}^{\rm open} - \theta_{kl}^{\rm open}| < 15°$ is required. Since each charged Higgs decays isotropically in its rest frame, in contrast to gluon radiation from quarks,

$$\cos\theta_{ij}^d \cdot \cos\theta_{kl}^d < 0.13 \tag{9}$$

is required.

The final-state topology varies widely as a function of Higgs mass, from being essentially two-jet-like with low sphericity and small average opening angle at low masses

to being nearly isotropic with high sphericity and large average opening angle at high masses. However, in the rest frame of each Higgs the topology is nearly two-jet-like with low sphericity throughout the accessible $H^{\pm}$ mass range, hence the boosted sphericity product $S^b_{ij} \cdot S^b_{kl}$ [20] is required to satisfy

$$S^b_{ij} \cdot S^b_{kl} < 0.03. \tag{10}$$

Since the two charged Higgs particles have the same velocities, the boosted sphericities should not be vastly different, and therefore

$$0.067 < S^b_{ij}/S^b_{kl} < 15.0 \tag{11}$$

is also required. With these selection criteria, six events are observed in the data, one with an average reconstructed mass of 25 GeV and the remaining five with average reconstructed masses > 40 GeV. Fig. 5 shows the quantity $S^b_{ij} \cdot S^b_{kl}$ for the data, the simulated background, and a simulated 30 GeV charged Higgs signal for those events which have a reconstructed average mass ± 2.5 GeV ($\simeq \pm\sigma_{\overline{M}}$) around 30 GeV and which pass all the selection criteria except $S^b_{ij} \cdot S^b_{kl} < 0.03$. The simulated background and the simulated charged Higgs signal are normalized to the integrated luminosity of the data.

Since there is no strong evidence for a signal in the accessible $H^{\pm}$ mass range, a 95% C.L. limit is set assuming Poisson statistics. At a given $M_{H^{\pm}}$, this limit is obtained by counting the number of events in the data (μ_o) in a region ± 2.5 GeV around $M_{H^{\pm}}$ which satisfy all selection criteria. The expected background is not subtracted, giving a more conservative limit. The contour of the excluded mass region is given in fig. 2 as a function of $BR[H^{\pm} \rightarrow cs]$ and in fig. 4 as a function of $BR[H^{\pm} \rightarrow cb]$, the hadronic branching ratios of the charged Higgs. Table 1 shows the number of expected signal (μ_s) and background (μ_b) events, the signal efficiency (ϵ) and μ_o for several values of $M_{H^{\pm}}$. The numbers μ_s, μ_b and μ_o are counted in a region ± 2.5 GeV around each value of $M_{H^{\pm}}$ in the table, in the same way as described at the end of section 4.

6 Results and Conclusions

Before making the limit contours, the following systematic errors are added in quadrature and subtracted from the expected signal for each channel: less than 2% systematic error in the luminosity measurement [24] and a 10% systematic error estimated from the effect of reasonable variations in the selection criteria. In addition, a 2.6% reduction in the signal for $H^+ H^- \to \nu\tau\ \nu\tau$ is made since the same percentage of the random trigger events are removed by the veto on ECAL or LCAL energy deposition described in section 3. Similarly, a 1.8% reduction in the signal for $H^+ H^- \to \nu\tau\ cs\,(\nu\tau\ c\bar{b})$ is made since the same percentage of random trigger events are removed by the requirements $E_{\rm LCAL} < 3$ GeV and $E_{\rm ECAL} < 35$ GeV described in section 4.

The individual limit contours for the decay channels $H^+ H^- \to \nu\bar{\tau}\ \bar{\nu}\tau$, $H^+ H^- \to \nu\tau\ cs\,(\nu\tau\ c\bar{b})$ and $H^+ H^- \to c\bar{s}\ \bar{c}s\,(c\bar{b}\ \bar{c}b)$ are shown in fig. 2 (4). All limits are obtained without the subtraction of expected background. Previous work has excluded the charged Higgs below 19 GeV [25]. In the analyses presented here, the lower limits on $M_{\rm H^\pm}$ are due to the following tendencies in the charged Higgs signatures which reduce the signal detection efficiencies: the increasing collinearity of the final state particles for $H^+ H^- \to \nu\bar{\tau}\ \bar{\nu}\tau$, the decreasing acoplanarity of the isolated charged particle for $H^+ H^- \to \nu\tau\ cs\,(\nu\tau\ c\bar{b})$, and the increasing two-jet-like behavior for $H^+ H^- \to c\bar{s}\ \bar{c}s\,(c\bar{b}\ \bar{c}b)$. The upper limits are due primarily to the decrease in production rate. The requirement that the angle between the jets $\theta_{\rm jets} < 135^\circ$ for $H^+ H^- \to \nu\tau\ cs\,(\nu\tau\ c\bar{b})$ and the difficulty in accurately reconstructing four jets for $H^+ H^- \to c\bar{s}\ \bar{c}s\,(c\bar{b}\ \bar{c}b)$ also reduce the signal detection efficiency for these decay channels at the larger values of $M_{\rm H^\pm}$.

To extend the limit outside the bounds described by the individual contours, the limits obtainable with any two or all three of the individual contours are calculated. This extended limit is found by using the sum of the number of observed events, $N_o^{\rm sum}$, and the sum of the expected signals, $\mu_s^{\rm sum}$, from the individual contours. The

combination of $N_o^{\rm sum}$ and $\mu_s^{\rm sum}$ giving the best limit on the branching ratio is used to make the combined contours shown by the heavier lines in figs. 2 and 4.

Fig. 2 indicates that at BR[$H^\pm \to \nu\tau$] = 100% the charged Higgs is excluded at 95% C.L. in the mass range 7.6 to 43.0 GeV, at BR[$H^\pm \to \nu\tau$] = BR[$H^\pm \to cs$] = 50% in the range 8.3 to 40.6 GeV and at BR[$H^\pm \to cs$] $\doteq$ 100% in the range 14.4 to 35.4 GeV. With cs replaced by cb, fig. 4 shows that at BR[$H^\pm \to \nu\tau$] = BR[$H^\pm \to cb$] = 50% the charged Higgs is excluded at 95% C.L. in the range 12.0 to 40.7 GeV, and at BR[$H^\pm \to cb$] = 100% in the range 16.2 to 35.7 GeV.

7 Acknowledgements

We would like to thank our colleagues of the LEP division for their outstanding performance in bringing the LEP machine into operation. Thanks also are due to the many engineering and technical personnel at CERN and at the home institutes for their contribution to ALEPH's success. Those of us not from member states wish to thank CERN for its hospitality.

References

[1] S.L. Glashow, Nucl. Phys. **A22** (1961) 579; S. Weinberg, Phys. Rev. Lett. **19** (1967) 1264; A. Salam, *Elementary Particle Theory*, ed. N. Svartholm, Stockholm, Almquist and Wiksell (1968), 367.

[2] P.W. Higgs, Phys. Lett. **12** (1964) 132; Phys. Rev. Lett. **13** (1964) 508; Phys. Rev. **145** (1966) 1156; F. Englert and R. Brout, Phys. Rev. Lett. **13** (1964) 321; G.S. Guralnik, C.R. Hagen and T.W.B. Kibble, Phys. Rev. Lett. **13** (1964) 585.

[3] G. Arnison *et. al.*, Phys. Lett. **126B** (1983) 398; P. Bagnaia *et. al.*, Phys. Lett. **129B** (1983) 130.

[4] D. Decamp *et. al.* (ALEPH Collaboration) Phys. Lett. **236B** (1990) 233; OPAL Collaboration, *Mass Limits for a Standard Model Higgs Boson in* e^+e^- *collisions at LEP*, CERN-EP/89-174 (1989); D. Decamp *et. al.* (ALEPH Collaboration) *Search for the Neutral Higgs Boson from* Z^0 *Decay in the Higgs Mass Range Between* 11 *and* 24 *GeV*, CERN-EP/90-016 (1990), submitted to Phys. Lett. B.

[5] T.D. Lee, Phys. Rev. **D8** (1973) 1226; S. Weinberg, Phys. Rev. Lett. **37** (1976) 657.

[6] R.D. Peccei and H.R. Quinn, Phys. Rev. Lett. **38** (1977) 1440 and Phys. Rev. **D16** (1977) 1791; S. Weinberg, Phys. Rev. Lett. **40** (1978) 223; F. Wilczek, Phys. Rev. Lett. **40** (1978) 279.

[7] P.B. Pal and L. Wolfenstein, Phys. Rev. **D25** (1982) 766 and references therein.

[8] S.L. Glashow and E.E. Jenkins, Phys. Lett. **196B** (1987) 233; P. Krawczyk and S. Pokorski, Phys. Rev. Lett. **60** (1988) 182; S. Nandi, Phys. Lett. **202B** (1988) 385; *Erratum:* **207B** (1988) 520;

[9] J. Wess and B. Zumino, Phys. Lett. **49B** (1974) 52. For reviews, see: H.-P. Nilles, Phys. Rep. bf 110C (1984) 1; C. Dounnas, A. Masiero, D.V. Nanopoulos and K.A. Olive, Grand Unification with and without supersymmetry and cosmological implications (World Scientific, Singapore, 1985); R. Arnowitt, A.H. Chamseddine and P. Nath, Applied $N = 1$ Supergravity (World Scientific, Singapore, 1985); J. Ellis, CERN-TH-4225 (1985).

[10] H. Baer *et. al.*, in *Physics at LEP*, CERN 86-02 Vol. 1, p. 332, eds. J. Ellis and R. Peccei; J. F. Gunion, H. E. Haber, G. L. Kane, and S. Dawson, *The Higgs Hunter's Guide* UCD 89-4; M. Drees *et. al.*, in *Z Physics at LEP*, CERN 89-08 Vol. 2 p. 91, eds. G. Altarelli, R. Kleiss, and C. Verzegnassi.

[11] M. Drees *et. al., op. cit.*, Vol. 2 p. 113.

[12] M. Drees *et. al., op. cit.*, Vol. 2 p. 114.

[13] J. Ellis, M.K. Gaillard, D.V. Nanopolous and P. Sikivie, Nucl. Phys. **B182** (1981) 529; J. Ellis, Lectures presented at the Les Houches Summer School (August 1981) LAPP-TH-48 and TH-3174-CERN.

[14] D. Decamp *et. al.* (ALEPH Collaboration), *ALEPH: A Detector for Electron-Positron Annihilations at LEP*, CERN-EP/90-025, submitted to Nucl. Inst. Meth.

[15] Particle Data Group, Phys. Lett. **204B** (1988).

[16] All hadronic processes were simulated with LUND 6.3 Parton Shower; M. Bengtsson and T. Sjöstrand, Phys. Lett. **185B** (1987) 435, and A. Peterson *et. al.*, Phys. Rev. **D37** (1988) 1. [This simulation has been shown to reproduce the data accurately: D. Decamp *et. al.* (ALEPH Collaboration), Phys. Lett. **234B** (1990) 209.]

[17] For electron-pair production the BABAMC Monte Carlo was used: M. Bohm, A. Denner, and W. Hollik, Nucl. Phys. **B304** (1988) 687, and F.A. Berends, R. Kleiss, and W.Hollik, Nucl. Phys. **B304** (1988) 712. For muon and tau pair production the KORALZ program was used: S. Jadach, *et. al., Z Physics at LEP1*, CERN Report 89-08 (1989), vol. III, p. 69 ff. For 2γ processes leading to $l^+l^-(\gamma)$ final states the program DIAG36 was used: F.A. Berends *et. al.* Nucl. Phys. **B253** (1985) 441. For 2γ processes leading to hadronic final states the PHOT01 Monte Carlo, based on the work of J. A. M. Vermasseren, with later contributions from S. Kawabata, J. Olsson, H. Wriedt, and J. M. Nye, was used.

[18] T. Sjöstrand, Comput. Phys. Comm. **28** (1983) 229. The LUCLUS algorithm with a d_{join} of 0.5 is used.

[19] T. Barklow, SLAC Report–315 (1987) 326.

[20] Sau Lan Wu, Nucl. Phys. **B3** (Proc. Suppl.) (1988) 102.

[21] T. Sjöstrand, *op. cit.* The LUCLUS algorithm with a $d_{\rm join}$ of 2.8 is used.

[22] T. Sjöstrand, *op. cit.* The LUCLUS algorithm with a $d_{\rm join}$ of 99999. is used.

[23] Sau Lan Wu, Z. Phys. **C9** (1981) 329.

[24] D. Decamp *et. al.* (ALEPH Collaboration), Phys. Lett. **235B** (1990) 399.

[25] A. Chen *et. al.* (CLEO Collaboration), Phys. Lett. **122B** (1983), 317; W. Bartel *et. al.* (JADE Collaboration), Z. Phys. **C31** (1986) 359; H.-J. Behrend *et. al.* (CELLO Collaboration), Phys. Lett. **193B** (1987) 376; S. M. Ritz, thesis, University of Wisconsin–Madison, Madison, Wisconsin, U.S.A., 1988.

Figure Captions

Fig. 1: The angle between the decay axes $\theta_{\mathbf{axes}}$ for the decay channel $H^+ H^- \to \nu\overline{\tau}\ \overline{\nu}\tau$ for the data, the simulated background, and a simulated 40.0 GeV charged Higgs signal for events which pass the 1-on-1 or 3-on-1 topology requirement and the invariant mass criteria. Both the simulated background and the simulated Higgs signal are normalized to the integrated luminosity of the data. Only events with $\theta_{\mathbf{axes}} < 154°$, as indicated by the arrow, are kept.

Fig. 2: The 95% C.L. limit on the mass of the charged Higgs as a function of BR[$H^\pm \to \nu\tau$] and BR[$H^\pm \to cs$]. The region on the hatched side of the contour is excluded. The combined limit for all channels is indicated by the heavier lines.

Fig. 3: The quantity p_t for the decay channel $H^+ H^- \to \nu\tau\ cs$ for the data, the simulated background, and a simulated 37.5 GeV charged Higgs signal for events which pass all selection criteria except $p_t > 6$ GeV. The simulated background and the simulated charged Higgs signal are normalized to the integrated luminosity of the data. Only events with $p_t > 6$ GeV, as indicated by the arrow, are kept.

Fig. 4: The 95% C.L. limit on the mass of the charged Higgs as a function of BR[$H^\pm \to \nu\tau$] and BR[$H^\pm \to cb$]. The region on the hatched side of the contour is excluded. The combined limit for all channels is indicated by the heavier lines.

Fig. 5: The boosted sphericity product $S^b_{ij} \cdot S^b_{kl}$ for the decay channel $H^+ H^- \to c\overline{s}\ \overline{c}s$ for the data, the simulated background, and a simulated 30.0 GeV charged Higgs signal for those events which have a reconstructed average mass ± 2.5 GeV ($\simeq \pm\sigma_{\overline{M}}$) around

30.0 GeV and which pass all the selection criteria except $S^b_{ij} \cdot S^b_{kl} < 0.03$. The simulated background and the simulated charged Higgs signal are normalized to the integrated luminosity of the data. Only events with $S^b_{ij} \cdot S^b_{kl} < 0.03$, as indicated by the arrow, are kept.

Table 1

Detection Efficiency and Number of Expected and Observed Events as a Function of Higgs Mass

	$H^+H^- \to \nu\bar{\tau}\,\bar{\nu}\tau$ [a]			$H^+H^- \to \nu\bar{\tau}\,\bar{c}s$ [b]			$H^+H^- \to c\bar{s}\,\bar{c}s$ [c]			
$M_{H^\pm}$ (GeV)	ϵ	μ_s	μ_b	ϵ	μ_s	μ_b	ϵ	μ_s	μ_o	μ_b
20	0.115	30.0	1.5	0.087	11.0	0.0	0.042	9.7	0	2.4
25	0.156	32.9	1.5	0.127	12.9	0.3	0.054	10.0	1	2.4
30	0.194	28.9	1.5	0.156	11.6	0.7	0.052	6.9	0	2.6
35	0.229	20.1	1.5	0.154	7.0	1.2	0.040	3.3	0	2.8
38	0.248	13.8	1.5	0.127	3.7	1.2	0.034	2.0	1	2.8
43	0.276	3.5	1.5	–	–	–	–	–	3	7.6
45	0.285	0.5	1.5	–	–	–	–	–	3	7.6

Note that for the decay channels $H^+H^- \to \nu\bar{\tau}\,\bar{\nu}\tau$ and $H^+H^- \to \nu\tau\,cs\,(\nu\tau\,cb)$ the number of observed events $\mu_o = 0$. In the table, ϵ is the signal detection efficiency, μ_s is the number of expected signal events, and μ_b is the number of expected background events.

[a] For $BR[H^\pm \to \nu\tau] = 100\%$.
[b] For $BR[H^\pm \to \nu\tau] = BR[H^\pm \to cs] = 50\%$.
[c] For $BR[H^\pm \to cs] = 100\%$.

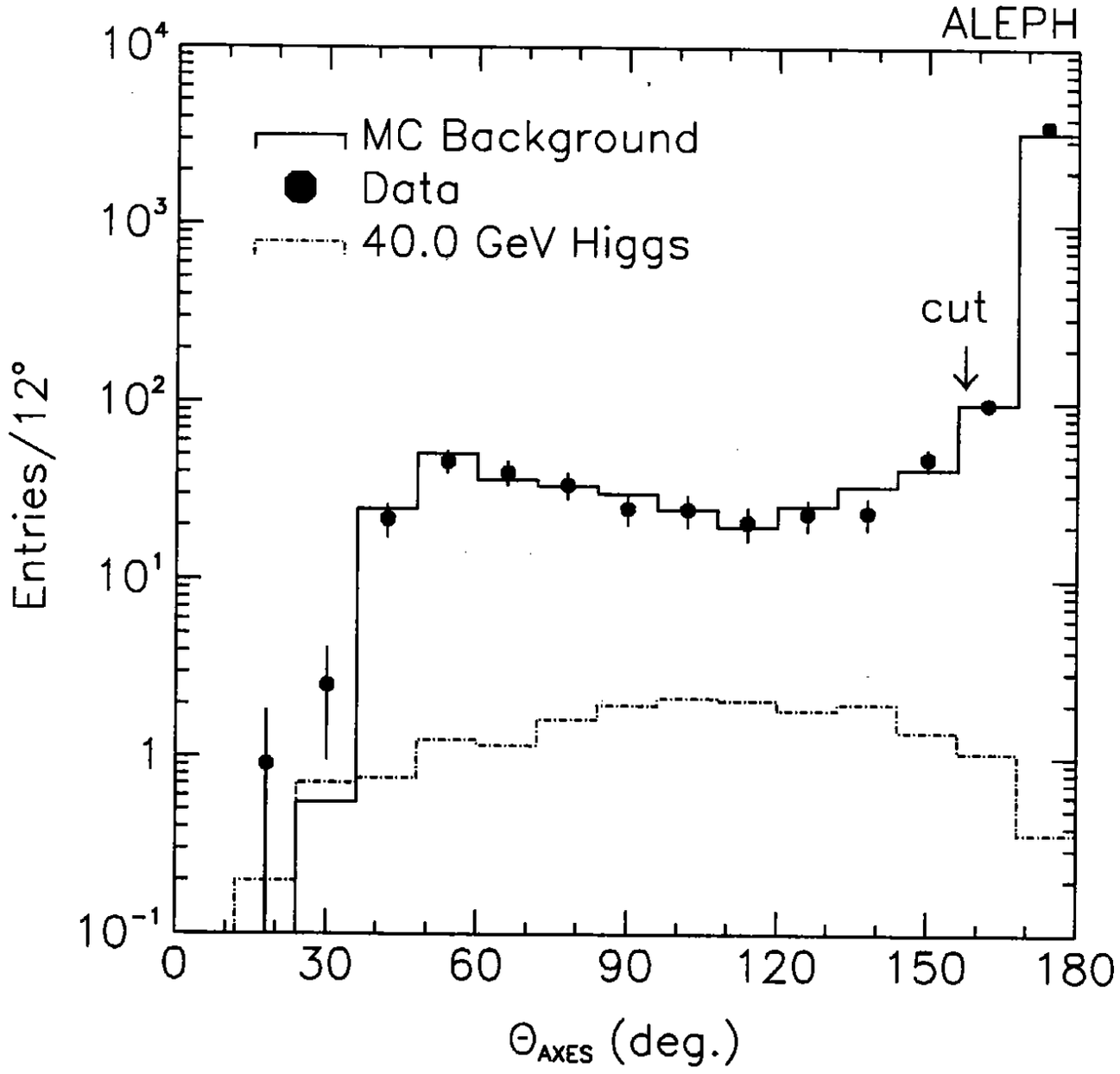
ALEPH
MC Background
Data
40.0 GeV Higgs
cut
Entries/12°
10^4
10^3
10^2
10^1
1
10^{-1}
0
30
60
90
120
150
180
Θ_{AXES} (deg.)

Fig. 1

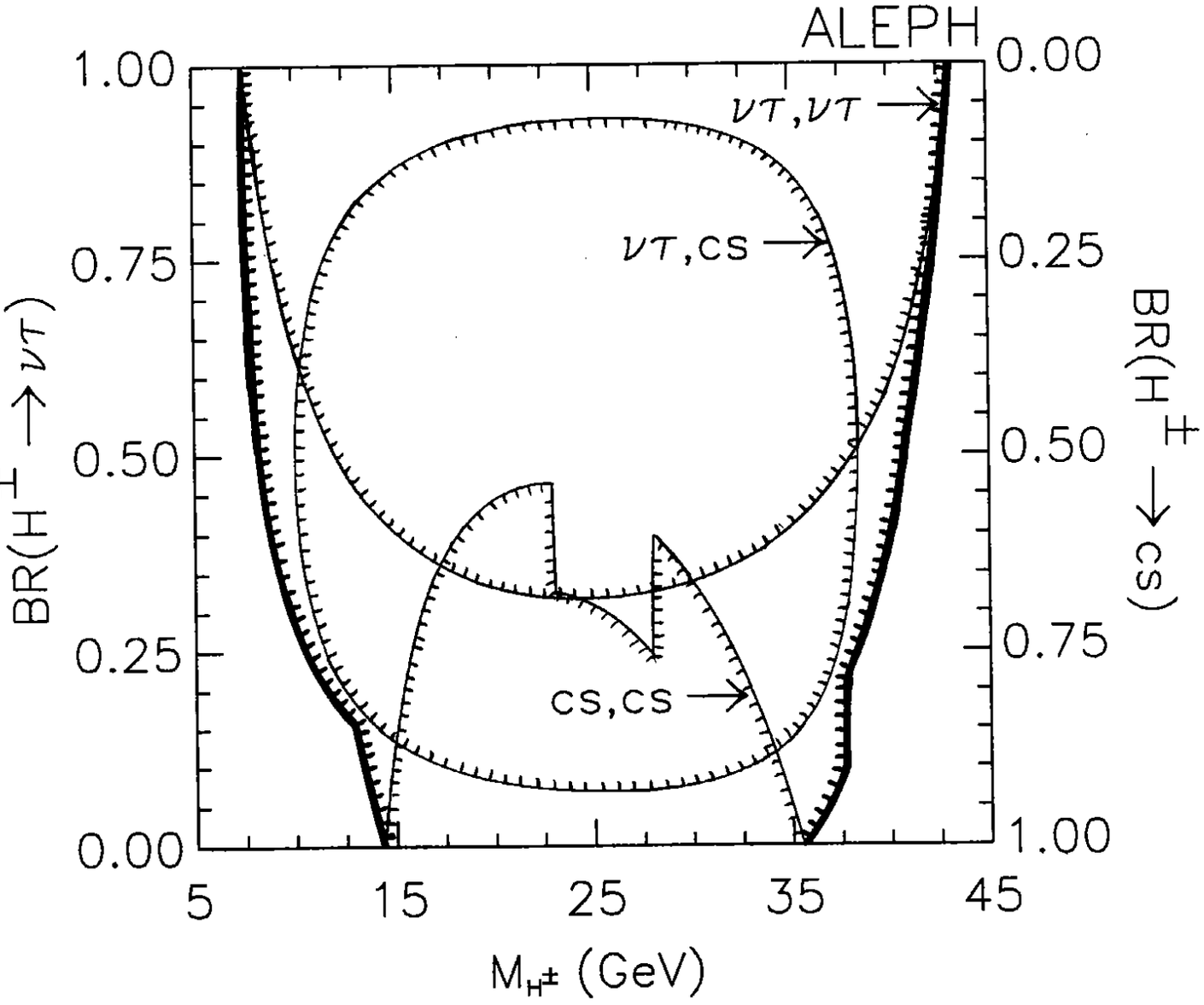
ALEPH
1.00
0.75
0.50
0.25
0.00
0.00
0.25
0.50
0.75
1.00
5
15
25
35
45
$M_{H^\pm}$ (GeV)
$BR(H^\pm \to \nu\tau)$
$BR(H^\pm \to cs)$
$\nu\tau,\nu\tau$
$\nu\tau,cs$
cs,cs

Fig. 2

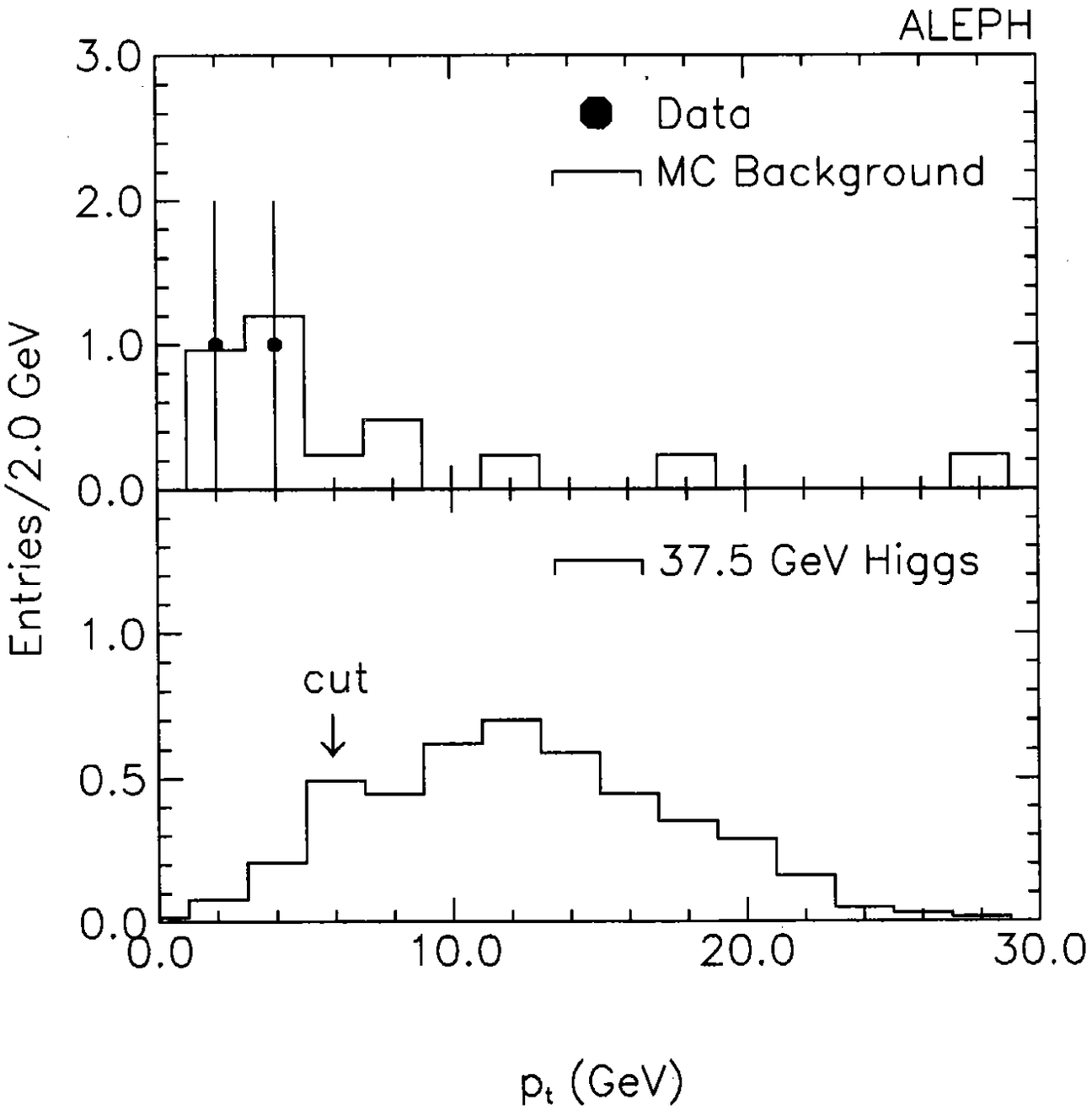
ALEPH
Data
MC Background
37.5 GeV Higgs
cut
Entries/2.0 GeV
3.0
2.0
1.0
0.0
1.0
0.5
0.0
0.0
10.0
20.0
30.0
p_t (GeV)

Fig. 3

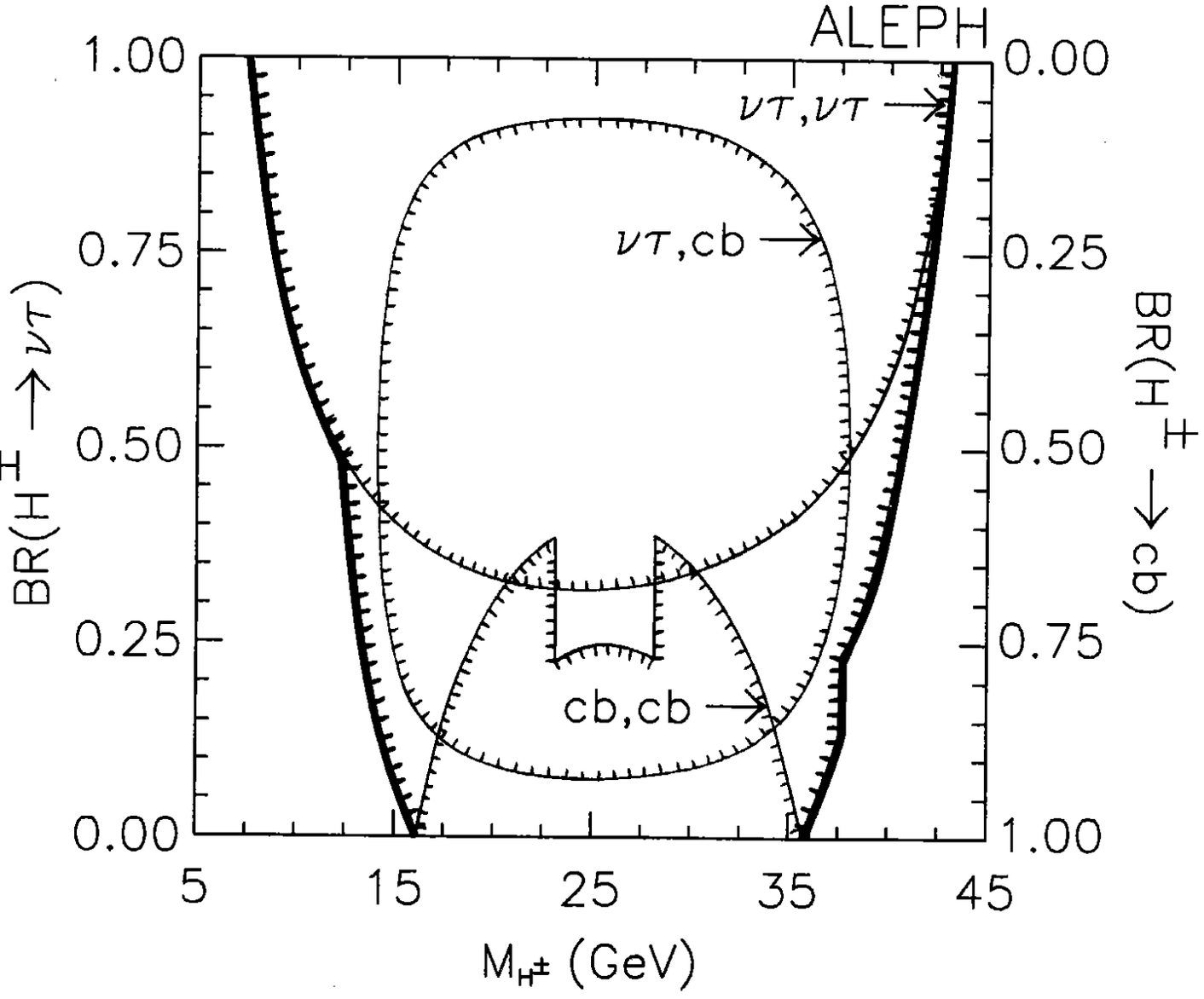
ALEPH
1.00
0.75
0.50
0.25
0.00
0.00
0.25
0.50
0.75
1.00
νT,νT
νT,cb
cb,cb
BR(H± → νT)
BR(H± → cb)
5
15
25
35
45
MH± (GeV)

Fig. 4

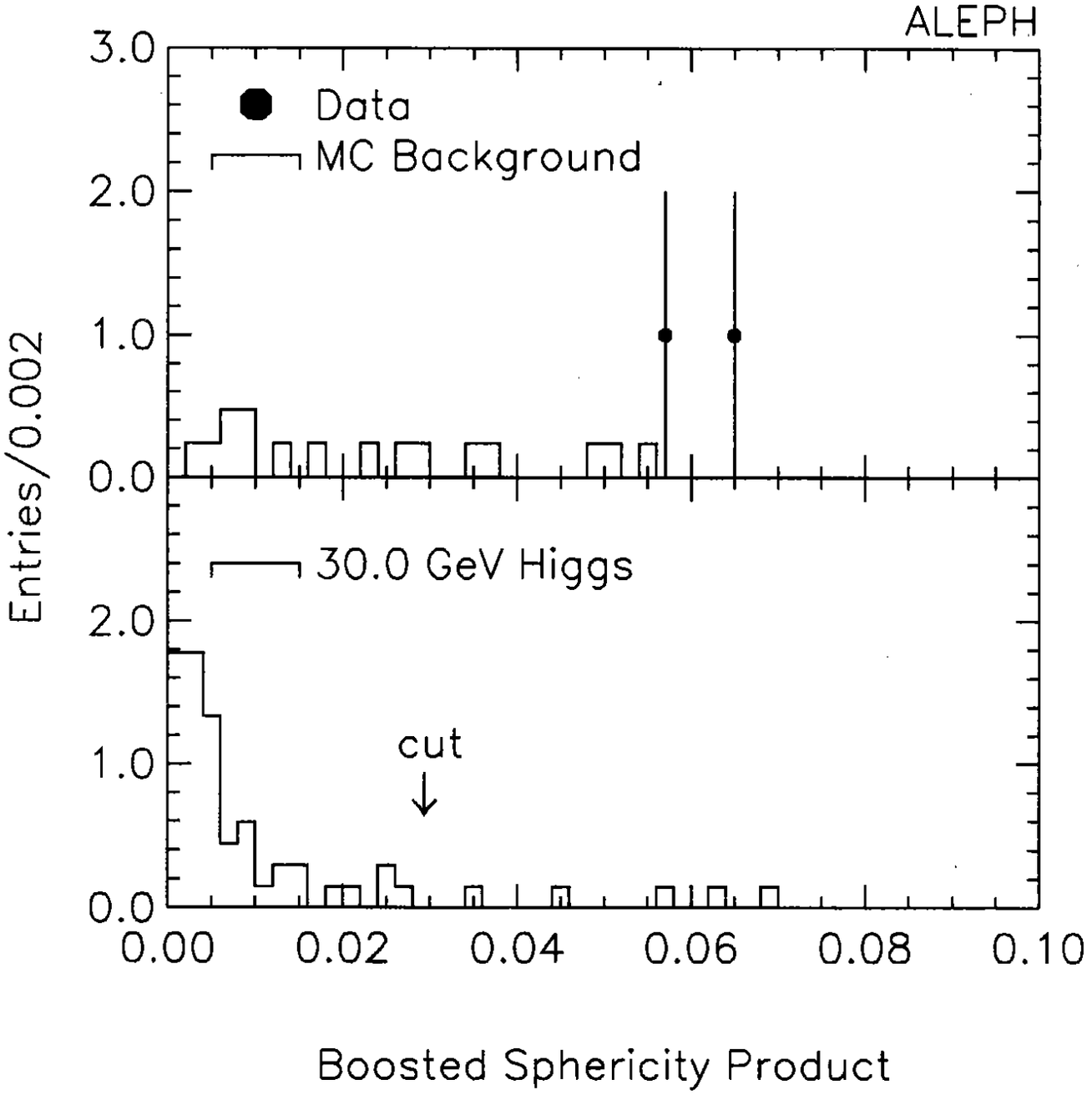
ALEPH
Data
MC Background
30.0 GeV Higgs
cut
Entries/0.002
Boosted Sphericity Product
3.0
2.0
1.0
0.0
0.00
0.02
0.04
0.06
0.08
0.10

Fig. 5